KeA1

CHINESE ROOTS
GLOBAL IMPACT

Contents lists available at ScienceDirect

Petroleum Science

journal homepage: www.keaipublishing.com/en/journals/petroleum-science



Original Paper

A novel dandelion-based bionic proppant and its transportation mechanism in different types of fractures



Jun Li ^{a, *}, Ming-Yi Wu ^b, Xu Han ^c, Si-Yuan He ^b, Ze-Yu Lin ^d

- a State Key Laboratory of Oil and Gas Reservoir Geology and Exploitation, Southwest Petroleum University, Chengdu, 610500, Sichuan, China
- ^b Sichuan Particles Energy and Technology Co., Ltd, Chengdu, 610599, Sichuan, China
- ^c Chongqing Industry Polytechnic College, Chongqing, 401120, China
- d Petroleum Systems Engineering, Faculty of Engineering and Applied Science, University of Regina, Regina, Saskatchewan, S4S 0A2, Canada

ARTICLE INFO

Article history: Received 10 June 2023 Received in revised form 31 January 2024 Accepted 1 February 2024 Available online 5 February 2024

Edited by Yan-Hua Sun

Keywords: Dandelion-based bionic proppant Low-viscosity fracturing fluid Unconventional reservoir Volumetric fracturing stimulation

ABSTRACT

Low-permeability reservoirs are generally characterized by low porosity and low permeability. Obtaining high production using the traditional method is technologically challenging because it yields a low reservoir recovery factor. In recent years, hydraulic fracturing technology is widely applied for efficiently exploiting and developing low-permeability reservoirs using a low-viscosity fluid as a fracturing fluid. However, the transportation of the proppant is inefficient in the low-viscosity fluid, and the proppant has a low piling-up height in fracture channels. These key challenges restrict the fluid (natural gas or oil) flow in fracture channels and their functional flow areas, reducing the profits of hydrocarbon exploitation. This study aimed to explore and develop a novel dandelion-bionic proppant by modifying the surface of the proppant and the fiber. Its structure was similar to that of dandelion seeds, and it had high transport and stacking efficiency in low-viscosity liquids compared with the traditional proppant.

Moreover, the transportation efficiency of this newly developed proppant was investigated experimentally using six different types of fracture models (tortuous fracture model, rough fracture model, narrow fracture model, complex fracture model, large-scale single fracture model, and small-scale single fracture model). Experimental results indicated that, compared with the traditional proppant, the transportation efficiency and the packing area of the dandelion-based bionic proppant significantly improved in tap water or low-viscosity fluid. Compared with the traditional proppant, the dandelion-based bionic proppant had 0.1–4 times longer transportation length, 0.3–5 times higher piling-up height, and 2–10 times larger placement area. The newly developed proppant also had some other extraordinary features. The tortuosity of the fracture did not influence the transportation of the novel proppant. This proppant could easily enter the branch fracture and narrow fracture with a high packing area in rough surface fractures. Based on the aforementioned characteristics, this novel proppant technique could improve the proppant transportation efficiency in the low-viscosity fracturing fluid and increase the ability of the proppant to enter the secondary fracture. This study might provide a new solution for effectively exploiting low-permeability hydrocarbon reservoirs.

© 2024 The Authors. Publishing services by Elsevier B.V. on behalf of KeAi Communications Co. Ltd. This is an open access article under the CC BY license (http://creativecommons.org/licenses/by/4.0/).

1. Introduction

The world is endowed with abundant low-permeability hydrocarbon reservoirs, including tight sandstone, shale oil, and shale gas. The economic development of low-permeability hydrocarbon reservoirs is essential to secure the energy supply (Li et al., 2020; Zou et al., 2015). Hydraulic fracturing technology paves the way for

* Corresponding author. E-mail address: lijunswpu@163.com (J. Li). the practical exploration of low-permeability reservoirs, commonly employing low-viscosity fluid (slickwater) as a fracturing fluid. Slickwater can reduce friction during the injection process and increase the complexity of fractures. However, it has low carrying and transportation abilities to the proppant. Thus, the proppant settles down quickly in the fracture and cannot easily enter the secondary fracture. In addition, the demerits of the slickwater carrying the proppant in hydraulic fracturing decrease the propped area of the fracture, reducing the valid stimulated volume. Therefore, the production of hydrocarbons is limited. Moreover, the proppant with slickwater is easily plugged at the wellbore or the

front of the fracture, increasing the operating costs and the risk of proppant blockage.

To address the aforementioned problem of low transportation efficiency of the proppant in the low-viscosity fracturing fluid and improve the proppant ability to enter the secondary fracture, two new types of the proppant have been proposed by scholars based on the properties of the proppant: the self-suspension proppant and the low-density proppant. The self-suspension proppant can be categorized into three types (Xu et al., 2021; Yao et al., 2021). The first type of self-suspension proppant is the water-soluble selfexpanding proppant. The surface of this proppant is covered with a layer of hydrogel, which expands after contact with water. The selfsuspending function is achieved by expanding the hydrogel, leading to an increase in the apparent volume of the proppant. Therefore, the lift force of the proppant is increased (Brian and Alan, 2015; Gol et al., 2017). However, the self-suspension proppant still has challenges in terms of moisture resistance, shear resistance, and temperature resistance. Notably, whether the proppant performs well at high temperatures or not and this performance still needs to be verified in practice. The second type of selfsuspension proppant is the viscoelastic proppant. The surface of this proppant is coated with a polymer, which is soluble in the fracturing fluid and increases the viscosity of the fracturing fluid. Thus, the suspending performance of the proppant is achieved (Fan et al., 2021; Zhou et al., 2022; Zoveidavianpoor and Gharibi, 2015). Similar to the first type of proppant, the viscoelastic proppant still has issues related to economic and formation damage. The third type of self-suspension proppant is the air-suspension proppant. The air-suspending function is fulfilled by the lifting force of the air attached to the proppant (Boyer et al., 2014; Darren et al., 2014; Kostenuk and Browne, 2010; Quintero et al., 2018; Zoveidavianpoor et al., 2018). However, whether or not the attachment between air bubbles and the proppant maintains stability in the fracturing fluid, which remain uncertain. Therefore, the air-suspension proppant still has issues. For example, the generation condition, distribution condition, and stability of the bubbles in formation situations (high temperature and pressure) still need to be ascertained.

Besides particle surface modification, the low-density proppant is commonly manufactured using the preferred new materials with low density. Therefore, the manufactured proppant has a relatively low density (Fan et al., 2018; Tasqué et al., 2020; Xie et al., 2019). Some low-density proppants have different structures than traditional proppants, which are designed as porous or hollow (Jones and Cutler, 1985; Li et al., 2018; Liao et al., 2021; Mou et al., 2017). However, the disadvantages of the low-density proppant are its relatively higher cost, high energy consumption, and complicated manufacturing process, which limit the popularization and application of the low-density proppant. Based on the aforementioned review, the performance of the self-suspension proppant still needs verification and improvisation, and the manufacturing cost and process of the low-density proppant still need optimization.

Given the limitations of the existing self-suspension proppants, this study mainly introduced a new proppant suitable for carrying in low-viscosity fluids. This proppant had the significant merits of high transport in the fracture and achieved better filling in longitudinal fractures. The first part of this study introduced the dandelion-based bionic proppant and its coupling, settling, and movement mechanisms. Then, the preparation and optimization of the proppant were implemented based on the investigated mechanism. In the second part, the material for the dandelion-based proppant was selected and optimized. Then, the settlement and transportation mechanisms of the dandelion-based bionic proppant in different types of fractures were discussed in the third and fourth parts. The last part of this study presented the conclusions.

2. Mechanisms of the dandelion-based bionic proppant

2.1. Coupling mechanisms of the dandelion-based bionic proppant

The fundamental idea of the dandelion-based bionic proppant was to mimic the fly performance of the dandelion, which consisted of the seeds and the pappus. The coupling mechanisms of this novel dandelion-based bionic proppant were explored in the early stages. Based on the current research, we found that the novel dandelion-based bionic proppant chemically adhered the proppant and the fiber together to construct a structure of dandelion seeds (seed + pappus, Fig. 1(a) and (c)). Based on our preliminary research, we speculated that the aforementioned chemical adherence was achieved through the attraction of charges. Specifically, a zwitterionic polymer was coated on the surface of the proppant, and a grafted cationic polymer was coated on the fiber. Thus, the proppant had positive and negative charges, whereas the fiber had a positive charge. The corresponding negative and positive charges on the surface gathered the modified group and created a stabilized structure (Fig. 1(b) and (d)). Thus, the charge anisotropy attraction helped construct the novel dandelion-based bionic proppant. However, this was only a preliminary result of the speculation that also discussed in a previous study (Li et al., 2022b). We continue to conduct further research on specific empirical evidence.

2.2. Settling mechanism of the dandelion-based bionic proppant

The modified proppant and modified fiber were coupled together to form a dandelion structure, which notably changed the settling mechanism of the proppant. The next part introduced the settling mechanism of the traditional proppant and the dandelion-based bionic proppant.

2.2.1. Settling mechanism of the traditional proppant

The traditional proppant could be assumed to be spherical. Its force analysis during the settlement in liquid is shown in Fig. 2(a). As depicted in the figure, the traditional proppant was affected by the fluid's gravity, buoyancy and resistance force also called viscous force. Assuming the traditional proppant was a regular sphere, the buoyancy and the viscous force were calculated using the buoyancy function and Navi—Stokes function (Eq. (1) and (2)), respectively.

$$F_{\rm b} = \rho_{\rm l} g V_{\rm p} \tag{1}$$

where F_b is the proppant buoyancy; ρ_l is the fluid density; g is the local gravitational acceleration; and V_p is the proppant volume.

$$F_{v} = 6\pi \eta_{1} r v \tag{2}$$

where $F_{\rm v}$ is the proppant viscous force; $\eta_{\rm l}$ is the viscous coefficient; r is the proppant diameter; and ν is the velocity of the proppant.

The force analysis showed that the interaction between the three forces influenced the settlement of the traditional proppant. The settling velocity was thus affected by these forces. The buoyancy and the gravity force were determined based on the basic properties of the traditional proppant. The traditional proppant accelerated downward at the beginning of the settlement and achieved an equilibrium velocity due to the viscous force. The proppant finally settled down to the bottom under the equilibrium velocity.

2.2.2. Settling mechanism of the dandelion-based bionic proppant

The apparent volume of the dandelion-based bionic proppant dramatically changed due to the coupling of the modified proppant and the fiber. As a result, the force analysis of the dandelion-based

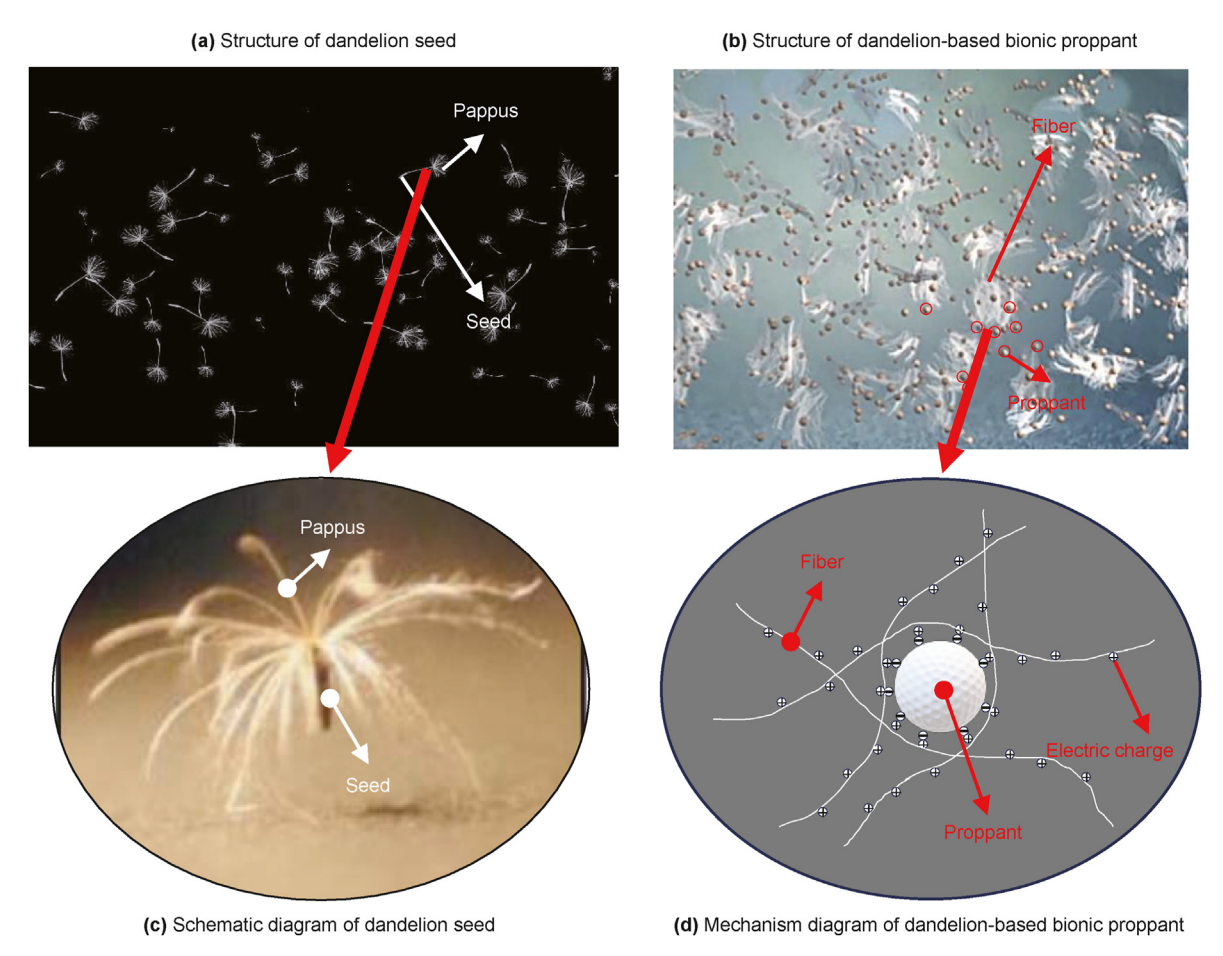


Fig. 1. Coupling mechanism of the dandelion-based bionic proppant.

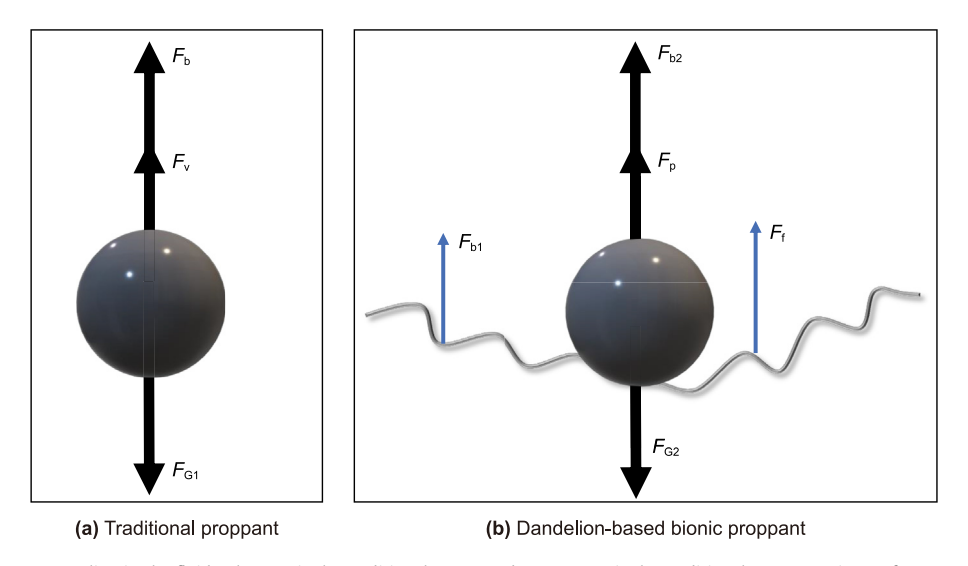


Fig. 2. Force analysis of proppant settling in the fluid, where F_b is the traditional proppant buoyancy, F_v is the traditional proppant viscous force, F_{G1} is the traditional proppant gravity, F_{b1} is the fiber buoyancy, F_{b2} is the modified proppant buoyancy, F_p is the viscous force of the modified proppant, F_f is the viscous force of the fiber, and F_{G2} is the dandelion-based bionic proppant gravity.

bionic proppant was also different. In addition, the randomness of the coupling complicated the structure of the coupled proppant and fiber, increasing the indeterminacy of the structure. However, the force analysis could still be conducted using a simplified structure, as shown in Fig. 2(b).

Despite the dandelion-based proppant having a structure different from that of the traditional proppant, its force analysis still included gravitational, buoyancy, and viscous forces. Among these forces, the gravitational force and the buoyancy of the dandelion-based proppant were calculated by adding those of the proppants

and fibers. Thus, the aforementioned force was not similar to that of the traditional proppant because the volume and mass of the fiber could not be neglected. However, after the proppant—fiber coupling, the apparent volume of the dandelion-based bionic proppant sharply increased. Thus, its viscous force increased, which was the most critical factor influencing the settlement of the proppant.

The viscous force of the dandelion-based bionic proppant could be divided into the viscous force of the proppant and the viscous force of the fiber. Therefore, the viscous force of the proppant and fiber was expressed as Eqs. (3) and (4), and the sphere's radius was equal to the radius of the proppant and fiber.

$$F_{\rm p} = 6\pi \eta_2 r_{\rm p} \nu \tag{3}$$

where F_p is the viscous force of the proppant; η_2 is the viscous coefficient of the fluid; and r_p is the equivalent radius.

$$F_{\rm f} = 6\pi \eta_{\rm I} r_{\rm f} \nu \tag{4}$$

where $F_{\rm f}$ is the viscous force of the fiber and $r_{\rm f}$ is the equivalent radius of the fiber.

Based on the aforementioned equation, the apparent volume of the dandelion-based bionic proppant was more significant than that of the traditional proppant. This contributed to a significant delay in the settlement of the proppant.

2.3. Transportation mechanism of the dandelion-based bionic proppant

Based on the aforementioned analysis of the settlement mechanism of the dandelion-based proppant, it was inferred that the settlement of the dandelion-based bionic proppant was delayed. Therefore, some exploratory experiments were conducted. As expected, the dandelion-based bionic proppant had a better carrying ability than the traditional proppant in the low-viscosity fluid due to the higher viscous force. Meanwhile, the dandelion-based bionic proppant had a lower settlement speed. Therefore, it could travel longer in fractures when carried by a low-viscosity fluid (Fig. 3(b)).

On the contrary, the traditional proppant settled down quickly once introduced into the fracture by the low-viscosity fluid, and then piled up in the front portion of the fracture (Fig. 3(a)). This study designed a series of experimental apparatuses to investigate the settlement and the movement mechanisms of the dandelion-based bionic proppant to verify the aforementioned assumptions.

The material selection and concentration optimization were conducted before the research on transportation mechanisms in different fracture types.

3. Material selection and optimization

The structure of the dandelion-based proppant was inspired by a bionic idea of coupling the proppant and the fiber. The coupling of the proppant and fiber was achieved by modifying the surface of the proppant and fiber. Thus, this study selected and optimized the modification material for the dandelion-based proppant.

3.1. Materials

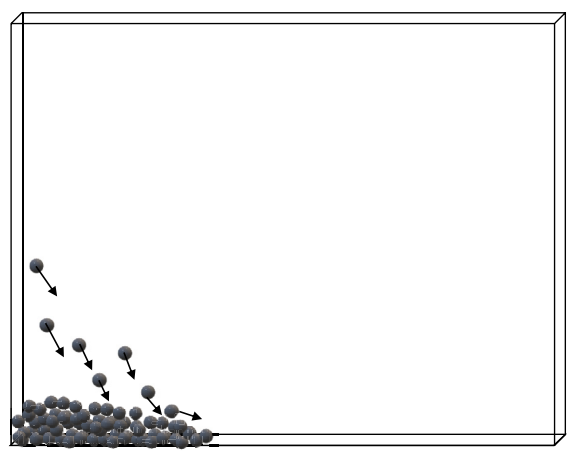
The dandelion-based bionic proppant was compatible with the slickwater in the experiment. The preparation method, surface characteristics test, and chemical modifier information were provided in a previous study (Li et al., 2022b). This study adopted the material and its preparation of the dandelion-based bionic proppant (Li et al., 2022b). A zwitterionic polymer (amino acid-type zwitterionic polymers and betaine-type zwitterionic polymers) was used to synthesize the proppant modifier, and a grafted cationic polymer (quaternary ammonium salt cationic polymer and amine salt cationic polymers) was used to synthesize the fiber modifier.

As presented in the previous study (Li et al., 2022b), the raw proppant (quartz sand) and the fiber were purchased from Ruiao China Co., Ltd. And Chaoshunyida China Co., Ltd., respectively. The raw material was also used as the traditional proppant for comparison. The particle size of the traditional proppant and the dandelion-based bionic proppant was 20/40 mesh. Their apparent densities were 2560 and 2480 kg/m³, respectively, and the roundness and sphericity ranged from 0.6 to 0.8. Moreover, the crushing rate and conductivity of the dandelion-based bionic proppant at 40 MPa were 6.8% and 77.2 µm³ cm, respectively, which were better than those of the traditional proppant. Table 1 lists the proppant parameters.

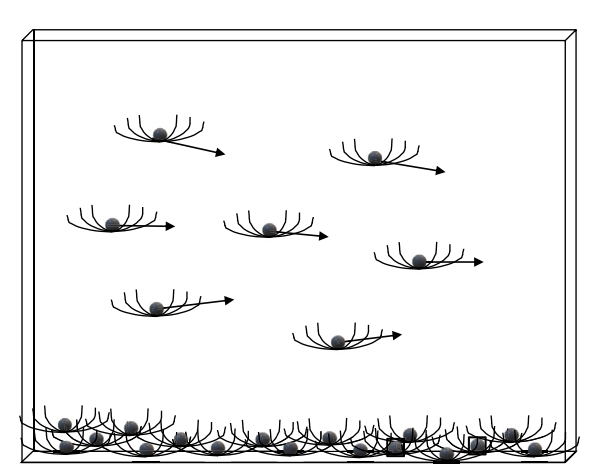
3.2. Experimental setup and procedures

3.2.1. Experimental setup of the material selection and optimization

A visual laboratory apparatus was designed to observe the coupling effect of the dandelion-based bionic proppant directly. As shown in Fig. 4, the apparatus consisted of a beaker, an agitator, and



(a) Traditional proppant



(b) Dandelion-based bionic proppant

Fig. 3. Transportation mechanism of the proppants.

Table 1 Proppant parameters.

Proppant type	Particle size, mesh	Density, kg/m ³	Sphericity	Roundness	Crushing rate @ 40 MPa, %	Conductivity @ 40 MPa, µm³ cm
Traditional proppant	20/40	2560	0.6-0.8	0.6-0.8	7.6	48.5
Dandelion-based bionic proppant	20/40	2480	0.6 - 0.8	0.6 - 0.8	6.8	77.2

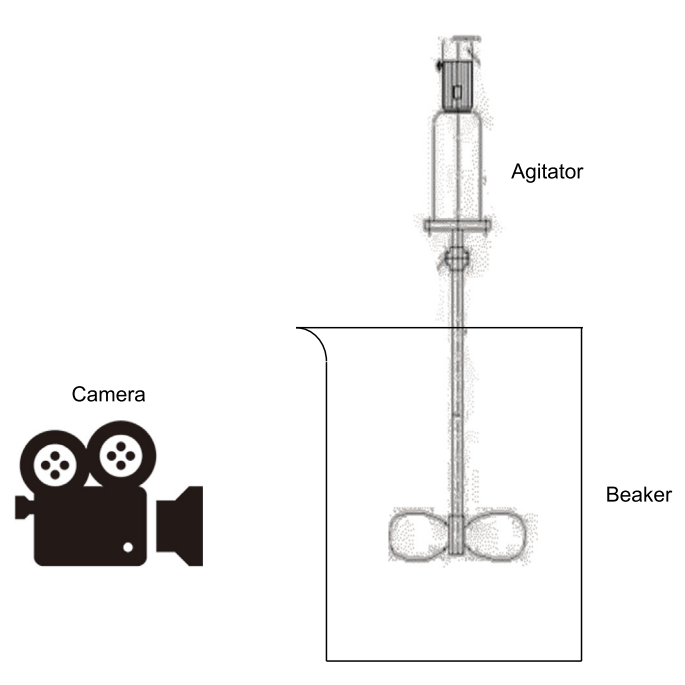


Fig. 4. Experimental setup of material selection and optimization of the dandelion-based bionic proppant.

a camera. Therefore, the coupling effect of different materials of the dandelion-based proppant was observed and optimized using the designed equipment.

3.2.2. Experimental procedures of the material selection and ontimization

Using the aforementioned apparatus, the material optimization of the dandelion-based proppant was performed as follows.

- (1) The dandelion-based bionic proppant was prepared, and 7.5 g of it was weighed.
- (2) Then, 250 g of the fracturing fluid was poured into a 500-mL beaker and the prepared proppant was placed in the same beaker.
- (3) An agitator was placed in the beaker and operated at a rotation speed of 800 rad/min for 30 s, during which the coupling effect of the dandelion-based bionic proppant was observed. A high-speed camera (East Fluid Measurement Technology (Beijing) Co., Ltd., 1920 × 1200 resolution, 2.3 million pixels) was used during the observation.
- (4) The aforementioned steps were repeated three times to obtain stable experimental results.

3.2.3. Experimental scheme of the material selection and optimization for the dandelion-based bionic proppant

Ten experiments were designed to select the fiber/proppant modifiers and optimize their concentrations. The optional proppant modifiers were PT1, PT2, and PT3 polymers at concentrations of 4%, 6%, and 8%, respectively. PT1 was an amino acid-type zwitterionic

polymer, whereas PT2 and PT3 were two types of betaine zwitterionic polymers. The optional fiber modifiers were FM1, FM2, and FM3 synthetic polymers at concentrations of 1%, 5%, and 9%, respectively (Table 2). Besides, FM1 was a quaternary ammonium salt cationic polymer, and FM2 and FM3 were two different types of amine salt cationic polymers. Noting that the dandelion-based bionic proppant was compatible with the low-viscosity fracturing fluid, the viscosity of the fracturing fluid was chosen to be 1–3 mPa s.

3.2.4. Evaluation criteria for the material selection and optimization

The dandelion-based bionic proppant had the characteristics of effectively coupling solid particles and soft fibers. Hence, the coupling effect was chosen as the evaluation criteria for the experimental results of the dandelion-based bionic proppant. In the experiment, the coupling effect was indicated by the proportion of the proppant suspension. The more significant the amount of the proppant suspended, the better the coupling effect. The material selection and concentration optimization were conducted based on these criteria.

3.3. Experimental results of material selection and optimization

3.3.1. Material selection for the proppant modifier

The coupling effects of the proppant with no modifier, modifier PT1, modifier PT2, and modifier PT3 were examined based on experiment sets 1–4 (Table 2). The results are shown in Fig. 5. Compared with the proppant with no modifier, the proppant with modifiers PT1, PT2, and PT3 showed some coupling effects with the fiber. However, the dandelion-based bionic proppant modified by PT2 was more likely to be suspended in the beaker and established a more stable coupling structure with the fiber (more proppant was in a suspended state). Therefore, PT2 was chosen as the proppant modifier.

3.3.2. Concentration optimization for the proppant modifier

The experiment tested the influence of the proppant modifier concentration on the coupling effect based on experiment sets 3, 5, and 6, as outlined in Table 2. The results are shown in Fig. 6. The test results indicated that the amount of suspended proppant in the beaker increased with the increase in the modifier concentration. The results suggested that a better coupling effect and stability of the dandelion-based bionic proppant were achieved with the use of the increased amount of modifier. However, increasing the amount of modifiers also increased the operation cost. The experiment on modifier concentration higher than 8% was not conducted considering the overall coupling effect and the cost of the dandelion-based bionic proppant.

3.3.3. Material selection for the fiber modifier

The optimization experiments on fiber modifiers were conducted based on experiment sets 6, 7, and 8, as outlined in Table 2. The results are shown in Fig. 7, revealing that the three fiber modifiers helped increase the proppant suspension performance. The experiments with FM2 and FM3 yielded similar results, and their coupling effect was superior to that of FM1. Considering the

 Table 2

 Experimental scheme of the material selection and optimization for the dandelion-based bionic proppant.

No.	Proppant mesh	Type of the proppant modifier	Concentration of the proppant modifier, %	Fiber modifier	Concentration of the fiber modifier, %
1	20/40	N/A	N/A	N/A	N/A
2	20/40	PT1	6	FM1	1
3	20/40	PT2	6	FM1	1
4	20/40	PT3	6	FM1	1
5	20/40	PT2	4	FM1	1
6	20/40	PT2	8	FM1	1
7	20/40	PT2	8	FM2	1
8	20/40	PT2	8	FM3	1
9	20/40	PT2	8	FM2	5
10	20/40	PT2	8	FM2	9

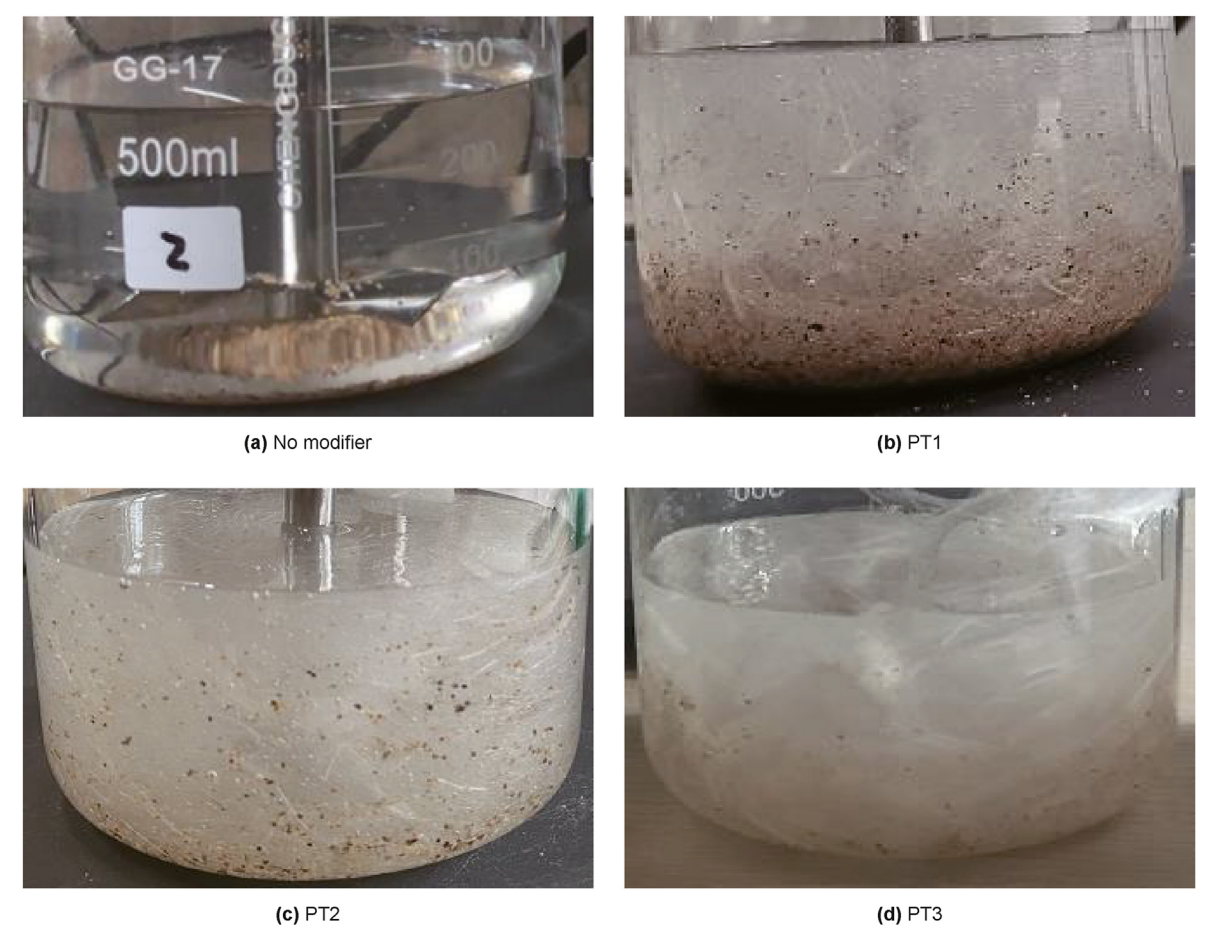


Fig. 5. Experimental results of the material selection for the proppant modifier.



Fig. 6. Experimental results of the concentration optimization of the proppant modifier PT2.

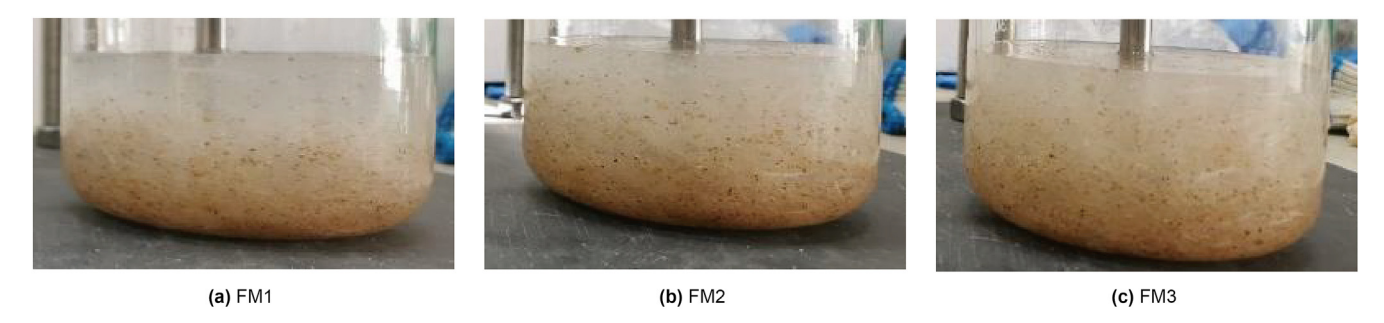


Fig. 7. Experimental results of the material selection for the fiber modifiers.

material costs and production safety, FM2 was selected as the fiber modifier.

3.3.4. Concentration optimization for the fiber modifier

Based on experiment sets 7, 9, and 10 outlined in Table 2, the experiments for optimizing fiber modifier concentration were conducted, as shown in Fig. 8. The results indicated that the amount of suspended proppant increased first and then decreased with the increase in the application of fiber modifiers to the proppant. It indicated that the coupling effect of the proppant and the fiber increased first and then decreased with the increase in the concentration of fiber modifier. Therefore, a 5% fiber modifier (FM2) concentration was selected.

4. Settlement of the dandelion-based bionic proppant

Based on the aforementioned analysis, it was postulated that the dandelion-based proppant had a prolonged settling time. Therefore, a settlement experiment was designed to verify the settlement performance of the dandelion-based bionic proppant and the traditional proppant. As mentioned earlier, given the structure complexity, we simplified the dandelion-based bionic proppant structure during settlement to a pair of single proppant and fiber (Fig. 9). Based on this simplified structure, we further investigated the structure of the dandelion-based bionic proppant and its classification to investigate its settlement characteristics in different conditions. The experimental materials used in this study are introduced in Section 2.1.

4.1. Experimental setup and procedures

4.1.1. Experimental setup of the settlement experiment

Fig. 10 illustrates the settlement experimental apparatus of the dandelion-based bionic proppant. A transparent acrylic bucket, 20 cm in diameter and 30 cm in height, was equipped with a ruler as a reference scale. The apparatus also comprised a high-speed camera and two LED (light emitting diode) light sources.

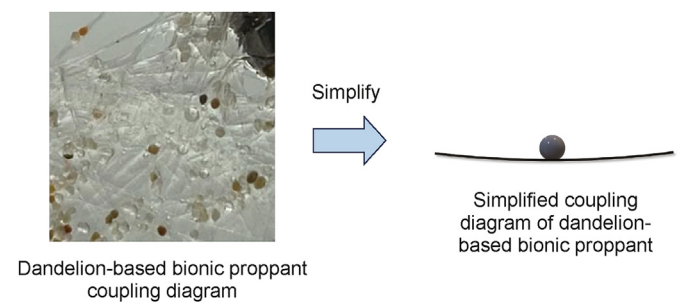


Fig. 9. Combination of the single fiber and proppant.

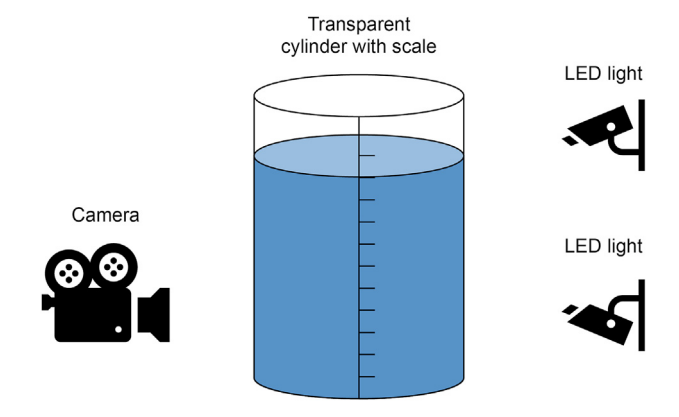


Fig. 10. Setup of the settlement experiment for the dandelion-based bionic proppant.

4.1.2. Procedures of the settlement experiment

Using the aforementioned experiment apparatus, we designed the procedures to study the settlement of the dandelion-based bionic proppant as follows.



Fig. 8. Experimental results of the concentration optimization for the fiber modifier FM2.

- 1) The dandelion-based bionic proppant was prepared.
- 2) The transparent bucket was filled up with water, and the positions of the high-speed camera and the light sources were adjusted to ensure the recording quality.
- 3) The camera was turned on, the proppant was allowed to drop from the water's surface, and the proppant settlement time was recorded. For each experiment, the procedure was repeated three times.

4.1.3. Scheme of the settlement experiment

Based on the aforementioned experimental procedures, the scheme of the settlement experiment was designed to investigate the difference between the dandelion-based bionic proppant and the traditional proppant (Table 3).

4.1.4. Evaluation criteria of settlement experiments

The most crucial feature of the dandelion-base bionic proppant was the settlement velocity. We used the high-speed camera to record the process. In this study, the proppant was dropped from static conditions at the same height. Therefore, the proppant settling time (from the water surface to the bottom) was recorded as an evaluation criterion.

4.2. Result of the settlement experiment

According to the experiment design outlined in Table 3, the settlement mechanism of single particles of dandelion-based bionic proppant and the traditional proppant in the 1 mPa s fluid was investigated. As shown in Fig. 11 The settling time of the dandelion-based bionic proppant was significantly longer than that of the traditional proppant in the low-viscosity fluid. The settling time of the dandelion-based bionic proppant was 2.25 times longer than that of the traditional proppant. The results indicated that the dandelion-based bionic proppant could delay the proppant settlement as anticipated. The settlement delay mechanism of the dandelion-based bionic proppant and its settlement process in the fluid will be explored in the following study.

5. Experiment of the dandelion-based bionic proppant transportation efficiency

The transportation efficiency of the dandelion-based bionic proppant was assessed based on settling and movement efficiency. Therefore, the proppant movement efficiency study was also of great significance. In this study, the visual fracture model was used to investigate the transportation of the proppant. The different types of fracture models were built to simulate the different fractures generated under complicated formation conditions. A comprehensive study of the transportation of the dandelion-based bionic proppant was conducted using different visual fracture models. The experimental materials are also introduced in Section 3.1.

5.1. Experimental setup and procedures

5.1.1. Setup of the proppant transportation experiment

Fig. 12 presents the experimental setup for the dandelion-based

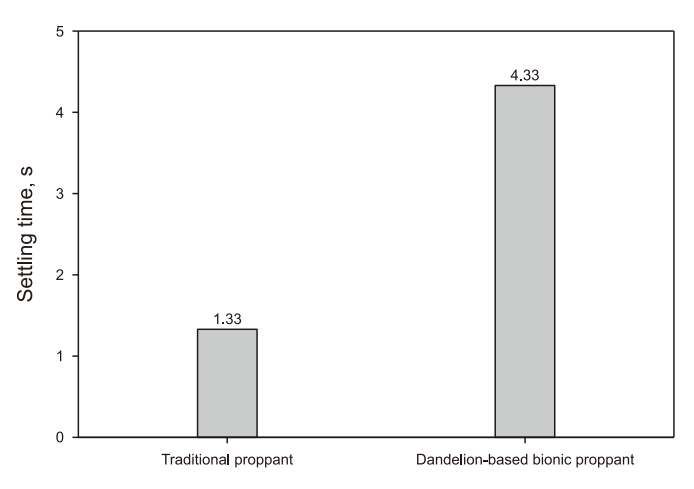


Fig. 11. Comparison of the settling time between the traditional proppant and the dandelion-based bionic proppant.

bionic proppant, comprising the control, mixing, injection, fracture, recycling, and data acquisition sectors. The fracture model was modularized and easily replaceable with a series of different types of fracture models to investigate the proppant transportation and movement in different types of fractures. Six typical fracture models were adopted in the experiment (small fracture model, tortuous fracture model, complex fracture model, large-scale fracture model, rough surface fracture model, and narrow fracture model).

The model parameter was acquired by the parameter conversion of the actual formation fracture based on the principle of similarity to ensure that the experiment had a similar operation condition as in the field. The underground Reynolds number in the field was assumed to be equal to the experimental Reynolds number of slurry, which also determined the injection rate (Eqs. (5) and (6)).

$$Q_1 S_2 = 2Q_2 S_1 \tag{5}$$

$$\begin{cases} Re_1 = Re_2 \\ Re_1 = \frac{\rho_1 \nu_1 l_1}{\mu_1} \\ Re_2 = \frac{\rho_2 \nu_2 l_2}{\mu_2} \end{cases}$$
 (6)

where Q_1 and Q_2 are pump rates in the field and physical model, respectively, cm³/s; S_1 and S_2 are the end fracture surface areas in the field and physical model, respectively, m²; Re_1 and Re_2 are the Reynolds number in the field and physical model, respectively; ρ_1 , and ρ_2 are the density of the fracturing fluid in the field and physical model, respectively, kg/m³; v_1 , v_2 are the velocities of the fracturing fluid in the field and physical model, respectively, m/s; μ_1 and μ_2 are the viscosity of the fracturing fluid in the field and physical model, respectively, Pa s; and l_1 and l_2 are the characteristic lengths in the field and physical model, respectively, m.

The formation properties could lead to different types of

Table 3Scheme of the settlement experiment.

No. Type of the proppant	Fiber length, mm	Fluid viscosity, mPa s
1 Traditional proppant 2 Dandelion-based bionic proppant	N/A 12	1 1

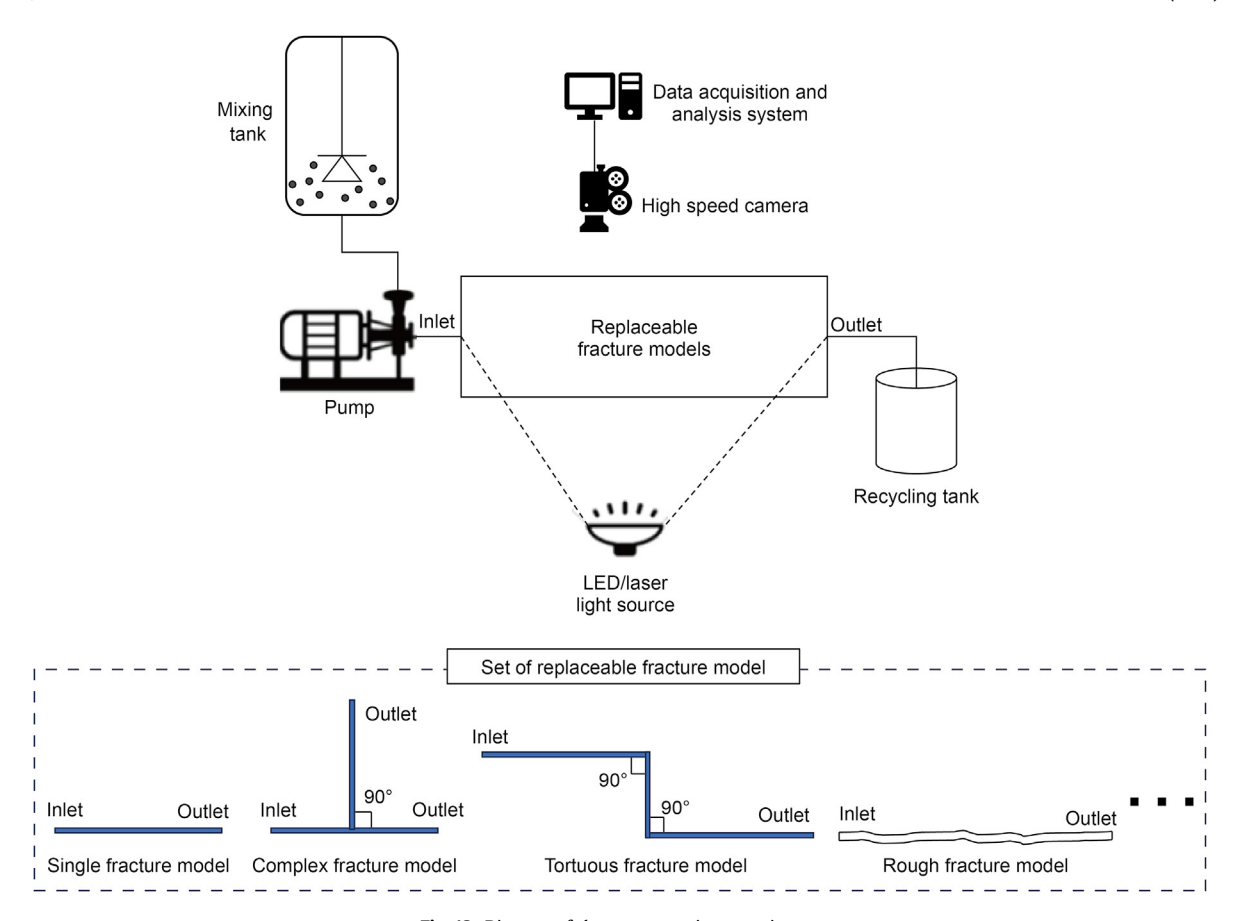


Fig. 12. Diagram of the transportation experiment.

artificial fractures during the fracturing process. As mentioned earlier, six types of fracture models were developed to simulate these typical fractures. The single fracture model was used to simulate one side of the biplane fracture, a configuration frequently studied by researchers. The configuration of the fracture model and its diagram are shown in Tables 4—9 and Fig. 13, respectively. The branch fracture model was used to simulate the complex fracture created by volumetric fracturing.

Besides, the 3D printing method was chosen to test the rough surface effect on dandelion-based bionic proppant transportation efficiency. The 3D printing technique was applied to build the rough surface fracture model to ensure the roughness and transparency of the model. The model-building steps are as follows.

- (1) A natural formation rock was cleaved to get the actual rough fracture surface.
- (2) The fracture rough surface was scanned and digitalized (Fig. 14).
- (3) The rough surface of the fracture was digitized, and its joint roughness coefficient (JRC) number was calculated. The optical surface was 3D-printed. (This study compared the difference in the proppant transportation in the rough surface and non-rough surface rather than quantitatively comparing

- the JRC.) Only a 3-mm depth of the rough surface was scanned and measured. The impact of the roughness on the transportation of the dandelion-based bionic proppant will also be explored in our subsequent study.
- (4) The rough fracture surface was placed in the parallel transparent plane to build the visual rough surface model.

5.1.2. Experimental procedures of the dandelion-based bionic proppant transportation

The experimental steps are as follows.

- (1) The fracture models were selected and assembled (single fracture model, tortuous fracture model, complex fracture model, large-scale fracture model, and narrow fracture model). The sealing of the experimental apparatus was checked.
- (2) The pre-flush fluid was prepared and mixed with dandelionbased bionic proppant.
- (3) The pump valve was opened to flush the fluid tank and the fracture inlet to fill the fracture model with the pre-flush fluid.

Table 4Transformation of the configurations of the small-scale single fracture model.

Fracture type	Fracture width	Fracture length	Fracture height	Fluid viscosity	Actual pump rate
Actual formation fracture	0.9 cm	145 m	80 m	1–10 cP	1–15 m³/min
Laboratory fracture model	0.9 cm	40 cm	22 cm	1–10 cP	23–344 cm³/s

Table 5Transformation of the configurations of the branch fracture model

Fracture type	Width of the main and secondary fractures	Length of the main fracture	Length of the secondary fracture	Fracture height	Angle of secondary fracture	Fluid viscosity	Actual pump rate
Actual formation fracture	0.9 cm	145 m	65 m	80 m	90°	1-10 cP	1–15 m ³ /min
Laboratory fracture model	0.9 cm	40 cm	18 cm	22 cm	90°	1-10 cP	23–344 cm ³ / s

Table 6Transformation of the configurations of the tortuous fracture model.

Fracture type	Fracture width	Fracture length	Fracture height	Fluid viscosity	Actual pump rate
Actual formation fracture	0.9 cm	190 m	80 m	1–10 cP	1–15 m³/min
Laboratory fracture model	0.9 cm	54 cm	22 cm	1–10 cP	23–344 cm³/s

Table 7Transformation of the configurations of the large-scale single fracture model.

Fracture type	Fracture width	Fracture length	Fracture height	Fluid viscosity	Actual pump rate
Actual formation fracture	0.9 cm	1000 m	125 m	1–10 cP	1–15 m ³ /min
Laboratory fracture model	0.9 cm	200 cm	25 cm	1–10 cP	17–250 cm ³ /s

Table 8Transformation of the configurations of the rough surface fracture model.

Fracture type	Fracture width	Fracture length	Fracture height	Fluid viscosity	Actual pump rate
Actual formation fracture	0.9 cm	70 m	35 m	1–10 cP	1–15 m ³ /min
Laboratory fracture model	0.9 cm	20 cm	10 cm	1–10 cP	23–350 cm ³ /s

Table 9Transformation of the configurations of the narrow fracture model.

Fracture type	Fracture width	Fracture length	Fracture height	Fluid viscosity	Actual pump rate
Actual formation fracture	0.3 cm	145 m	80 m	1–10 cP	1–15 m ³ /min
Laboratory fracture model	0.3 cm	40 cm	22 cm	1–10 cP	23–344 cm ³ /s

- (4) The pre-flush fluid tank valve was closed, and the mixing tank and pump valve were opened to inject the dandelion-based bionic proppant into the fracture.
- (5) The transportation process of the dandelion-based bionic propapant was recorded in the different types of fracture models.

5.1.3. Experimental scheme of the proppant transportation

Thirteen sets of the proppant placement and transportation experiments were designed (Table 10) to better differentiate the transportation mechanisms of the dandelion-based bionic proppant from those of the traditional proppant in different types of fracture models. The added mass of proppant was 125 g. The length of the fiber was 3 mm, and the concentration of the fiber was 1% for the dandelion-based bionic proppant. The model inlet was set in the middle, and the viscosity of the fracturing fluid was 1–3 cP. The detailed information is provided in Table 10.

5.1.4. Evaluation criteria of the dandelion-based bionic proppant transportation experiment

The experimental results included pictures and videos. The videos were used to record the movement of the proppant during the experiment, and the pictures of the final packing pattern of

proppants were used to acquire the digitalized characteristic parameters with the software. Four parameters were chosen to evaluate the proppant placement: (1) equilibrium height, which was the height of the proppant dune when particles reached equilibrium conditions; (2) length of the proppant dune, which was the longest distance that the proppant could reach; and (3) placement area of the proppant dune, which was the total area of the proppant placed in the fracture. Eq. (7) was used to calculate the proppant placement area. The conductive channel rate was a dimensionless parameter as mentioned in the previous study (Li et al., 2022b). Therefore, to achieve higher proppant transportation efficiency, it is essential to increase the proppant transportation distance, enhance the packing height, enlarge the packing area, and elevate the conductive channel rate (Fernández et al., 2015; Hu et al., 2018; Li et al., 2017).

$$S = \int_0^l f(x) \mathrm{d}x \tag{7}$$

where S is the area of the proppant dune; I is the length of the proppant dune; and f(x) is the relationship between the proppant height and length.

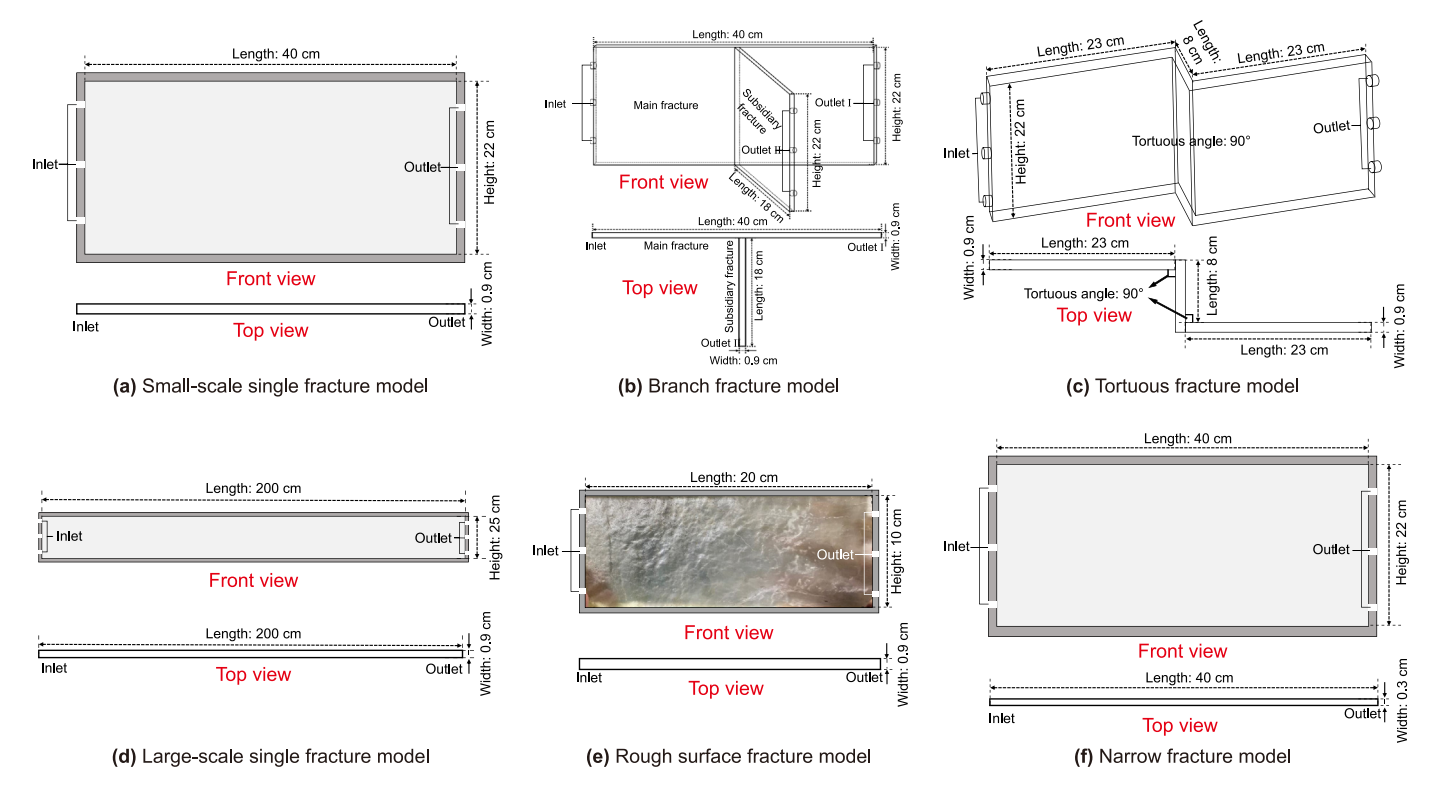


Fig. 13. Diagram of different types of fracture models.

5.2. Experimental results of the dandelion-based bionic proppant transportation in fractures

5.2.1. Experimental results of the dandelion-based bionic proppant transportation in a small-scale single fracture

The transportation and its difference between the traditional proppant, the combination of the traditional proppant and traditional fiber, and the dandelion-based bionic proppant in the single fracture were investigated based on experiment sets 1–3 (Table 10). The transportation process is shown in Fig. 15. The parameters of the different proppant dunes are shown in Fig. 16. As depicted in Fig. 15(a), the transportation of the traditional proppant in the single fracture mainly depended on the fluid-carrying capacity. The proppant settled down quickly after entering the fracture model, ultimately forming a tight triangle proppant dune. This configuration resulted in a limited propped area for the traditional proppant, as shown in Fig. 16. Other researchers also obtained a similar result (Hu et al., 2018; Zhang et al., 2017). For the experiment of combining the traditional proppant and the traditional fiber in a low-viscosity fracturing fluid, the introduction of traditional fiber did not influence the transportation of the traditional proppant. The traditional proppant also settled down quickly in the fracture, and most of the traditional fiber was separated in the fluid. The traditional fiber floated on the top of the fracture (increasing the risk of plugging), and the traditional proppant piled up at the bottom of the fracture (Fig. 15(b)). Fig. 15(c) shows that the dandelion-based bionic proppant had a sound coupling effect between the proppant and the fiber, which formed a porous spongelike structure in the fracture. The coupled proppant and fiber mainly floated in the fracture. Moreover, after the settlement of the dandelion-based bionic proppant, a crafted structure was established that increased the conductivity of the fracture.

Comparing the parameters of the traditional proppant and combining the traditional proppant and the traditional fiber

(Fig. 16(a)), a significant improvement was observed in the final packing height and the effective propped area of the dandelionbased bionic proppant. The packing height doubled compared with the traditional proppant, and the final placement was four times larger than that for the traditional proppant. The results proved that the transportation performance of the dandelion-based bionic proppant in a single fracture model dramatically improved. The final channel rate of the dandelion-based bionic proppant reached 55%, compared with the 2% channel rate of the combination of the traditional proppant and the traditional fiber. The traditional proppant stacked at the bottom of the fracture due to the gravity effect. The formed proppant dune had nearly no channels for fluid flow. On introducing the traditional fiber into the traditional proppant, only narrow channels were observed on the surface of the proppant dune. The channels were not connected, impeding the fluid flow. A new type of pilling-up structure was established for the dandelion-based bionic proppant due to the sound coupling effect. The proppant was supported by the crafted fiber, losing the proppant dune and creating flow channels in centimeter scale. Meanwhile, the channels were connected throughout the whole proppant dune. Therefore, we speculated that the new piling-up structure provided opened flow channels for the hydrocarbons and improved the conductivity of the fracture.

5.2.2. Experimental results of the dandelion-based bionic proppant transportation in branch fracture

Based on experiment sets 4 and 5 outlined in Table 10, the movement and direction-changing ability of the dandelion-based bionic proppant and the traditional proppant in the 90° branch fracture model were investigated. Figs. 17 and 18 illustrate the parameters of the final proppant dune. The height and placement area of the dandelion-based bionic proppant were far greater than those of the traditional proppant in the main fracture, as shown in Figs. 17 and 18. Li et al. (2017) and Xiao et al. (2021) reported that

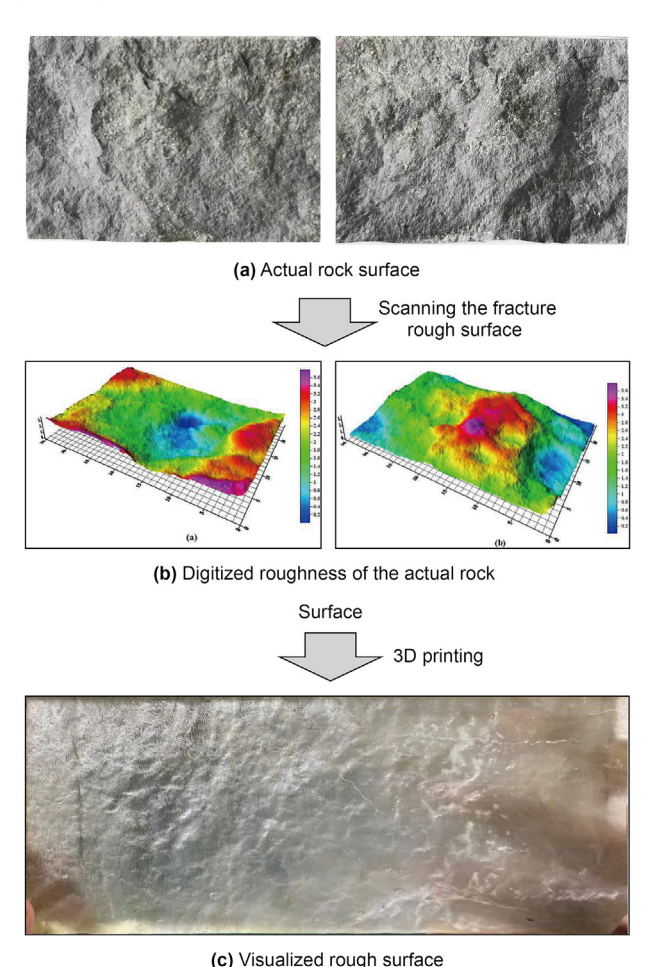


Fig. 14. Process of constructing the visualized rough surface using 3D printing technology based on the actual rock surfaces.

the pump rate and viscosity of the fracturing fluid significantly influenced the transportation of the traditional proppant. More proppant was transported in the secondary fracture at a higher pump rate and a higher fluid viscosity. However, the pump rate and fluid viscosity in this study were relatively small, which had less influence on the proppant entering the secondary fracture (Fig. 17(a)). On comparing the experimental results, it was found that the transportation length, height, and placement area of the dandelion-based bionic proppant in the main fracture were 1.5, 3, and 5 times larger than those of the traditional proppant,

respectively. Meanwhile, the transportation length, height, and placement area of the dandelion-based bionic proppant in the branch fracture were 4, 5.5, and 7 times larger than those of the traditional proppant. Compared with the traditional proppant, the placement area of the dandelion-based bionic proppant in the branch area showed the best improvement, implying that the dandelion-based bionic proppant had a better direction-changing ability to enter the branch fracture from the main fracture.

5.2.3. Experimental results of the dandelion-based bionic proppant transportation in the tortuous fracture

Experiment sets 6 and 7 outlined in Table 10 investigated the transportation efficiency of the dandelion-based bionic proppant and the traditional proppant in the 90° tortuous fracture model. Previous studies (Ou et al. 2021a, 2021b) demonstrated the transportation of the traditional proppant in a 90° tortuous fracture, revealing a gently descending curve that corresponded to the experimental results shown in Fig. 19. However, the placement of the dandelion-based bionic proppant differed from that of the traditional proppant, which showed an uneven sponge-like pattern. The experimental results were not directly observed in a single view due to the tortuosity of the fracture model. Hence, the pattern of the final proppant dune presented in Fig. 19 was the combination of the experimental results recorded from multiple views (the front and side views). The tortuous fracture section in the middle of the fracture model is shown in Fig. 19 (as marked in the red box). The comparison of the proppant dune parameter between the traditional proppant and the dandelion-based bionic proppant in a 90° tortuous fracture model is shown in Fig. 20. It was observed that the height and the packing area of the dandelionbased bionic proppant were doubled than those of the traditional proppant. However, due to the limitation of the fracture model, the lengths of the proppant dune of traditional proppant and the dandelion-based bionic proppant were the same. However, on comparing the repose angle of the proppant dune, it was observed that the repose angle of the traditional proppant was acute (6°) whereas that of the dandelion-based bionic proppant was obtuse angle (157°) (Fig. 19). Indicating the better transportation efficiency of the dandelion-based bionic proppant in the tortuous fracture. In other words, the unique movement efficiency of the dandelionbased bionic proppant led to minor interference by the tortuosity of the fracture, leading to better movement abilities.

5.2.4. Experimental results of the dandelion-based bionic proppant transportation in the rough surface fracture

Based on experiment sets 8 and 9 outlined in Table 10, the transportation of the dandelion-based bionic proppant and the traditional proppant in the rough surface fracture was examined.

Table 10 Experimental scheme of different types of fracture models.

No.	Fracture type	Pump rate, cm ³ /s	Proppant concentration, g	Proppant size, mesh	Proppant type
1	Small-scale single fracture	70	125	20/40	Traditional proppant
2	Small-scale single fracture	70	125	20/40	Traditional proppant $+$ traditional fiber
3	Small-scale single fracture	70	125	20/40	Dandelion-based bionic proppant
4	90° branch fracture	70	125	20/40	Traditional proppant
5	90° branch fracture	70	125	20/40	Dandelion-based bionic proppant
6	90° tortuous fracture	70	125	20/40	Traditional proppant
7	90° tortuous fracture	70	125	20/40	Dandelion-based bionic proppant
8	Rough surface fracture	70	125	20/40	Traditional proppant
9	Rough surface fracture	70	125	20/40	Dandelion-based bionic proppant
10	Large-scale single fracture	70	625	20/40	Traditional proppant
11	Large-scale single fracture	70	625	20/40	Dandelion-based bionic proppant
12	3-mm narrow fracture	70	125	20/40	Traditional proppant
13	3-mm narrow fracture	70	125	20/40	Dandelion-based bionic proppant

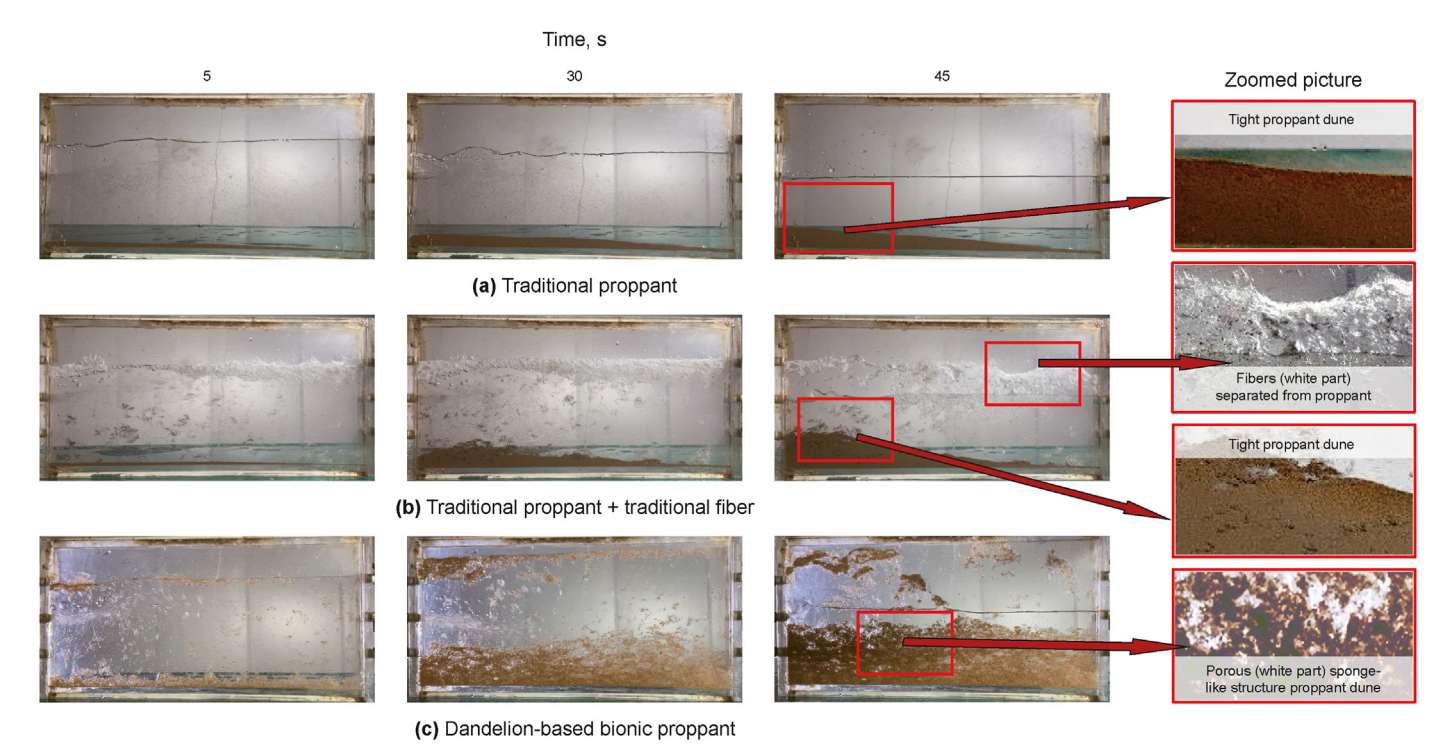


Fig. 15. The packing pattern of the proppant dune changes over time in a small-scale single fracture model.

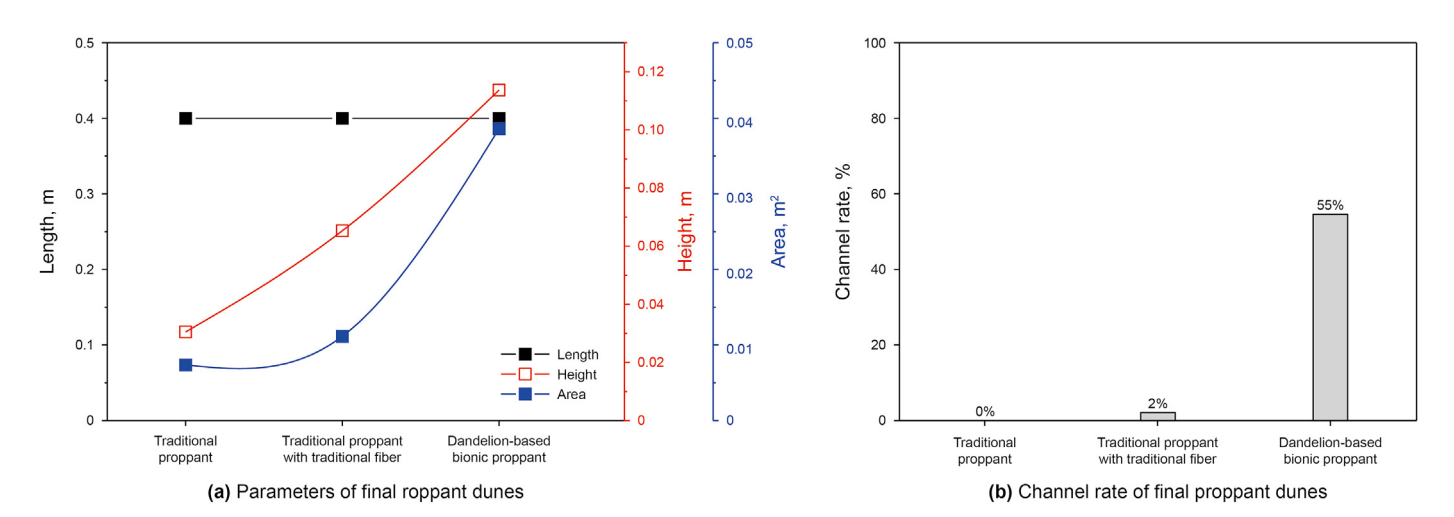


Fig. 16. Parameters and flow channel rate of the proppant dune of different types of the proppant in the small-scale single fracture model.

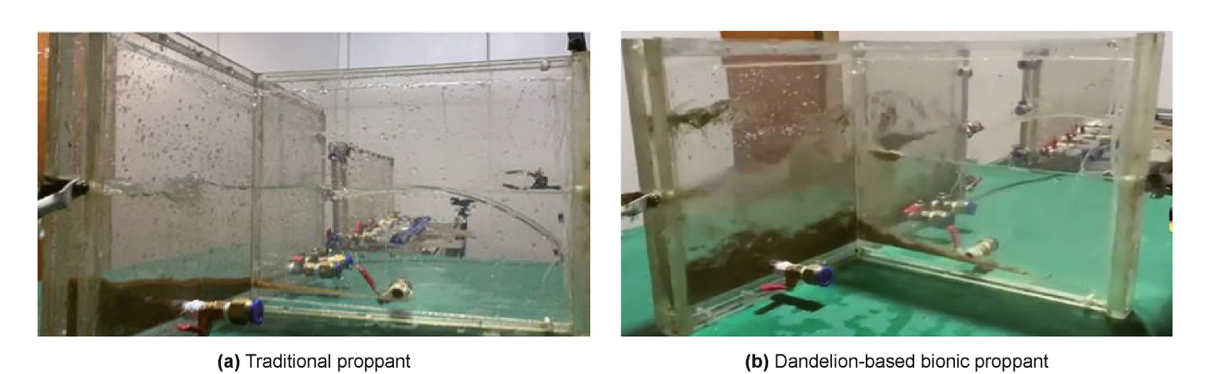


Fig. 17. Final packing pattern of traditional proppant and dandelion-based bionic proppant in the 90° branch fracture model.

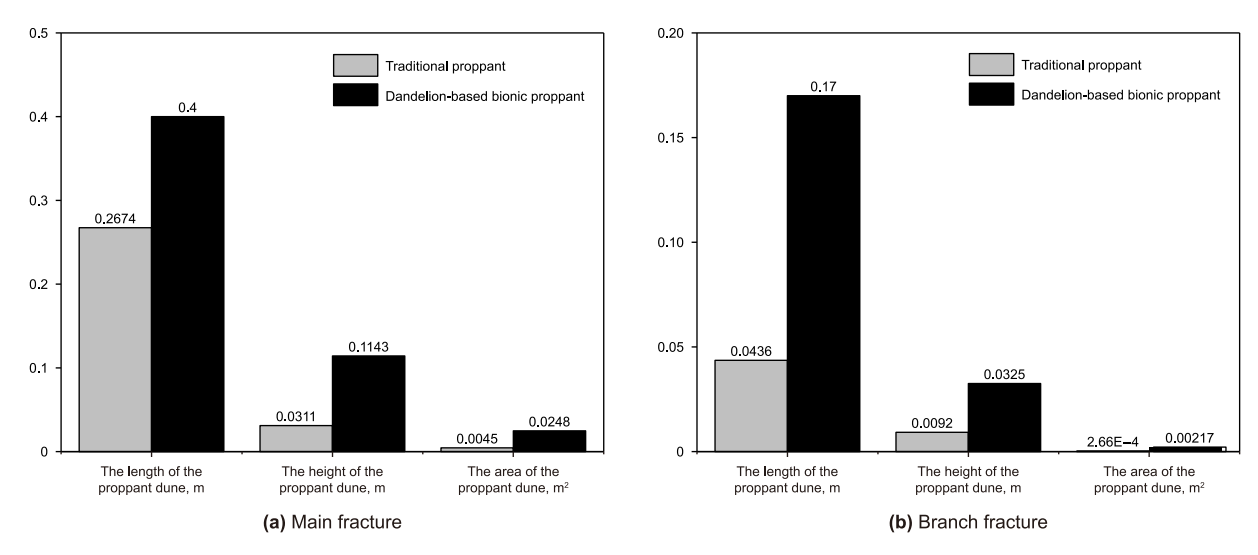


Fig. 18. Comparisons of proppant dune parameters between the traditional proppant and dandelion-based bionic proppant in the main fracture and the branch fracture of 90° branch fracture model.

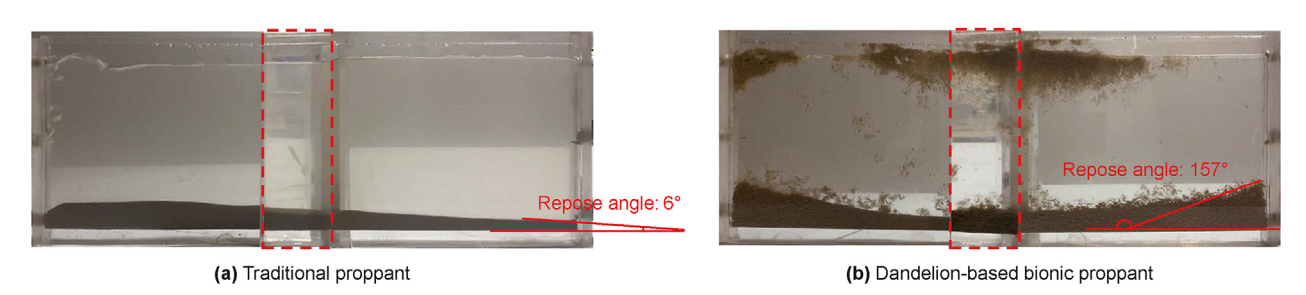


Fig. 19. Proppant dune and repose angle of traditional proppant and dandelion-based bionic proppant (middle part is a tortuous corner) in a 90° tortuous fracture model.

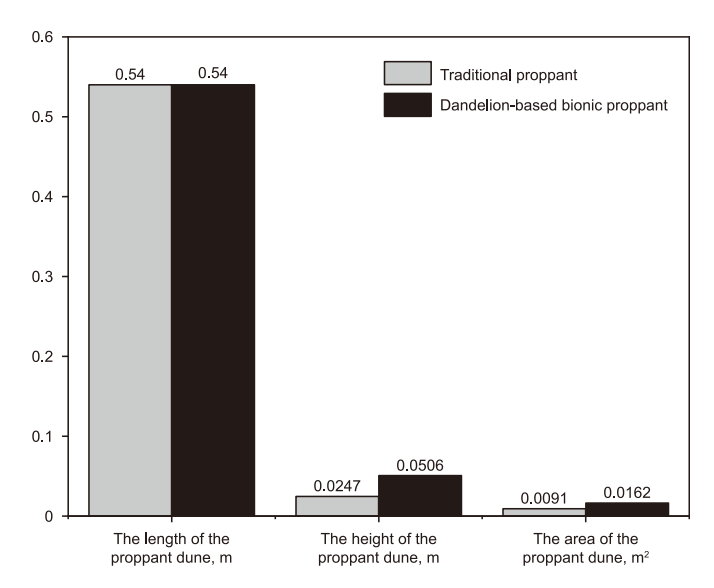


Fig. 20. Comparisons of proppant dune parameters between the traditional proppant and the dandelion-based bionic proppant in a 90° tortuous fracture model.

The final results of the proppant dune are shown in Figs. 21 and 22. The experimental results showed that the collision between the traditional proppant and the fracture surface was weak, leading to the quick settlement of the traditional proppant after entering from the model inlet. The placement pattern of the traditional proppant

displayed a short triangle, which was supported by other researchers (Huang et al., 2017; Li et al., 2021). However, the particular structure of the dandelion-based bionic proppant intensified the collision between the proppant and the rough surface, improving its transportation efficiency and the placement area in rough surface fractures. Comparison of the parameter of the proppant dune shown in Fig. 22 showed that the length, height, and placement area of the dandelion-based bionic proppant were 1.5, 3, and 10 times greater than those of the traditional proppant. The placement area of the dandelion-based bionic proppant was only four times bigger than that of the traditional proppant in a straight small-scale fracture model, indicating better improvement in the transportation efficiency of the dandelion-based bionic proppant in the rough surface fractures. Also, the rough surface delayed the settlement of the dandelion-based bionic proppant. Some of the proppants even adhered to the rough surface, improving the placement efficiency (placement area and height) of the dandelionbased bionic proppant.

5.2.5. Experimental results of the dandelion-based bionic proppant transportation in the large-scale fracture

Experiment sets 10 and 11 outlined in Table 10 were designed to examine the influence of the large-scale fracture model on the transportation of the dandelion-based bionic proppant. The final pattern of the proppant dune is shown in Figs. 23 and 24. The results showed that the transportation length, piling-up height, and placement area of the dandelion-based bionic proppant in the large-scale fracture model were better than those of the traditional proppant, which improved by 60%, 30%, and 220%, respectively. The

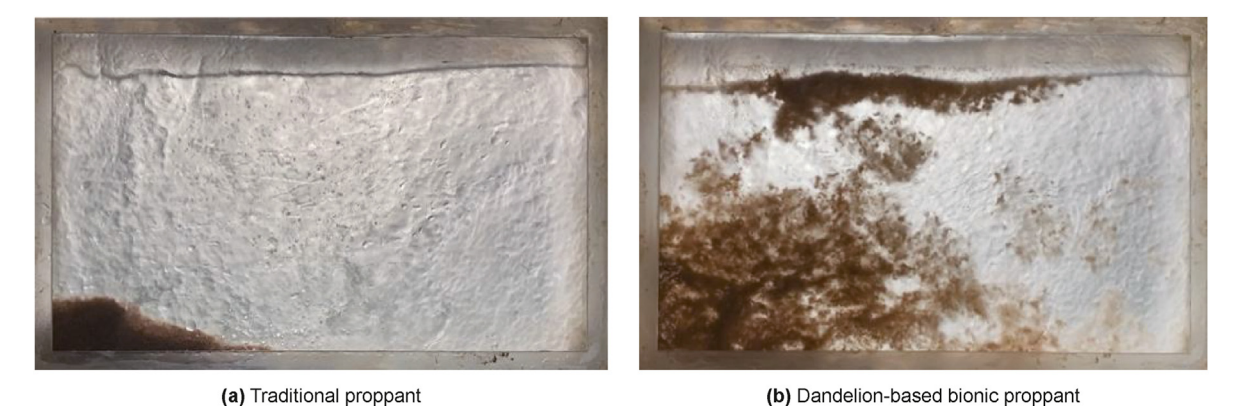


Fig. 21. Proppant dune of traditional proppant and dandelion-based bionic proppant in the rough surface fracture model.

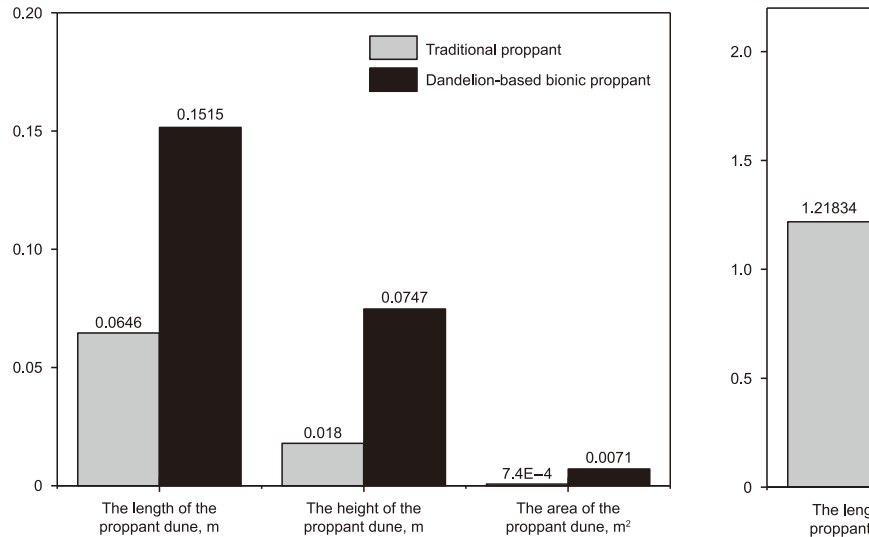


Fig. 22. Comparisons of proppant dune parameters between the traditional proppant and the dandelion-based bionic proppant in the rough fracture model.

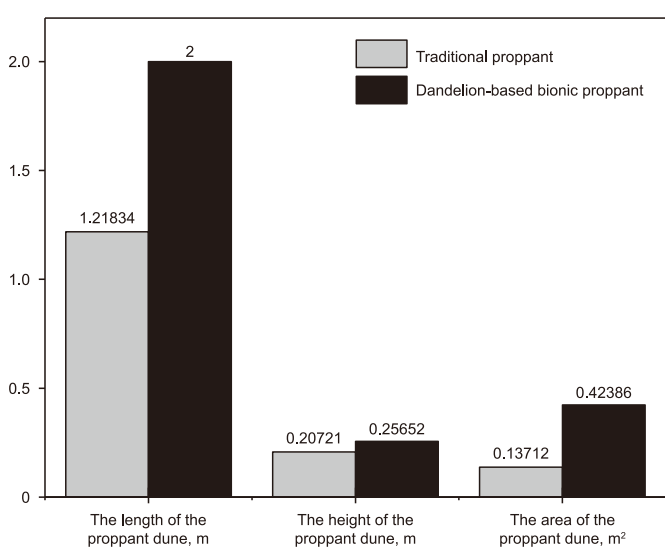


Fig. 24. Comparisons of proppant dune parameters between the traditional proppant and the dandelion-based bionic proppant in a large-scale fracture model.



Fig. 23. Proppant dune and its zoomed picture of traditional proppant and dandelion-based bionic proppant in a large-scale fracture model.

experimental results indicated that the dandelion-based bionic proppant was not influenced by the scale of the fracture, inferring an excellent transportation efficiency of the dandelion-based bionic proppant in actual hydraulic fractures. As shown in Fig. 23, the

zoomed pictures of the final proppant dune illustrated that the traditional proppant dune was tight without visible flow channels; similar observations were reported by Li et al. (2022a) and Wen et al. (2016). The proppant dune of the dandelion-based bionic



(a) Traditional proppant

(b) Dandelion-based bionic proppant

Fig. 25. Packing pattern of traditional proppant and dandelion-based bionic proppant in a 3-mm-narrow width of the fracture model.

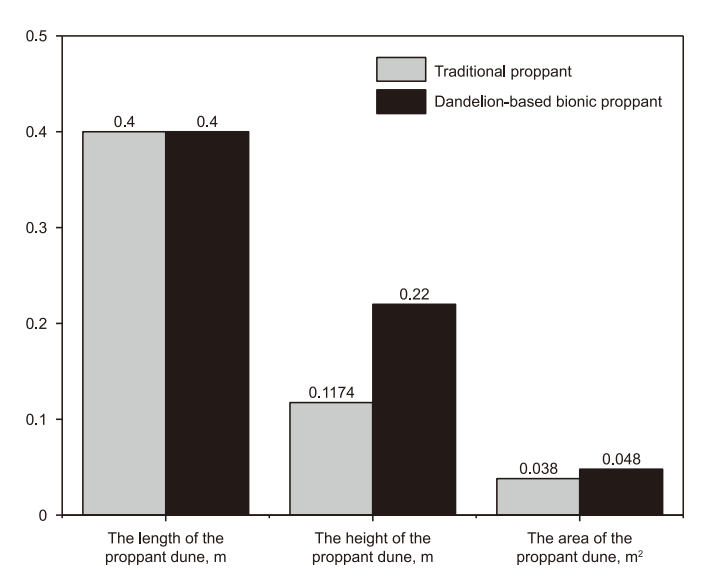


Fig. 26. Comparisons of proppant dune parameters between the traditional proppant and the dandelion-based bionic proppant in a 3-mm-narrow width of the fracture model

proppant was loose. Moreover, centimeter-scale pores and channels were observed in the proppant dune, confirming that the coupling effect of the dandelion-based bionic proppant was not changed using the magnified large-scale fractures.

5.2.6. Experimental results of the dandelion-based bionic proppant transportation in the narrow width of the fracture

Experiment sets 12 and 13 outlined in Table 10 were used to examine the transportation efficiency of the dandelion-based bionic proppant and the traditional proppant transportation in the narrow width of fracture models. The final patterns of the proppant dune are shown in Figs. 25 and 26. The experimental results illustrated that the dandelion-based bionic proppant could also efficiently couple and form a proppant dune with large channels in the narrow fracture (Fig. 25). It was observed that the height and the packing area of the dandelion-based bionic proppant were also larger than those of the traditional proppant. Besides, the lengths of the traditional proppant and the dandelion-based bionic proppant were equal due to the limitation of the fracture model (Fig. 26).

6. Conclusions

This study developed a novel dandelion-based bionic proppant, which had high transportation efficiency in a low-viscosity fluid and established high-conductivity flow channels. The conclusions were presented by conducting material selection, material optimization study, and study of the different types of proppant transportation in different types of fracture models.

- The optimized proppant modifier concentration was 8% of PT2, and the optimized fiber modifier concentration was 5% of FM2.
- (2) The dandelion-based bionic proppant was floating in the fracturing fluid, and the settlement of the dandelion-based bionic proppant, a crafted structure could be established. Hence, the proppant dune formed by the dandelion-based bionic proppant had larger flow channels.
- (3) The settling time of the dandelion-based bionic proppant was longer than that of the traditional proppant.
- (4) The dandelion-based bionic proppant had a unique movement mode in the fluid. Compared with the traditional proppant, the transportation distance of the proppant in different types of fractures increased by about 0.1–4 times, the stacking height increased by about 0.3–5 times, and the placement area increased by about 2–10 times.
- (5) The dandelion-based bionic proppant could more readily transport in the tortuous fractures, deviate into the branch fractures, and enter into the narrow width of fractures. Compared with the traditional proppant, the dandelionbased bionic proppant had less impact on transportation when encountering tortuous fracture, narrow fracture, and branch fracture. At the same time, the rough fracture could also improve the placement efficiency of the dandelionbased bionic proppant.

CRediT authorship contribution statement

Jun Li: Conceptualization, Investigation, Methodology, Writing — original draft, Writing — review & editing. **Ming-Yi Wu:** Data curation, Investigation, Methodology. **Xu Han:** Investigation. **Si-Yuan He:** Investigation, Visualization. **Ze-Yu Lin:** Investigation, Writing — review & editing.

Declaration of competing interest

The authors declare that they have no known competing financial interests or personal relationships that could have appeared to influence the work reported in this paper.

Acknowledgments

This study was supported by the Natural Science Foundation of Sichuan "Settlement and Transport Mechanism of Biomimetic Dandelion Proppant in Fracture" (No. 23NSFSC5596) and the China Postdoctoral Science Foundation (No. 2023M742904).

References

- Boyer, J., Maley, D., O'Neil, B., 2014. Chemically enhanced proppant transport. In:

 SPE Annual Technical Conference and Exhibition. https://doi.org/10.2118/
- Brian, G., Alan, V., 2015. Self-suspending proppant transport technology increases stimulated reservoir volume and reduces proppant pack and formation damage. In: SPE Annual Technical Conference and Exhibition. https://doi.org/ 10.2118/174867-MS.
- Darren, M., Jeff, B., Bill, O.N., 2014. Surface modification of proppant to improve transport and placement. In: International Petroleum Technology Conference 2014. https://doi.org/10.2523/IPTC-17806-MS.
- Fan, F., Li, F., Tian, S., Sheng, M., Khan, W., Shi, A., Zhou, Y., Xu, Q., 2021. Hydrophobic epoxy resin coated proppants with ultra-high self-suspension ability and enhanced liquid conductivity. Petrol. Sci. 18, 1753–1759. https://doi.org/ 10.1016/j.petsci.2021.09.004.
- Fan, J.M., Bailey, T.P., Sun, Z.Q., Zhao, P.C., Uher, C., Yuan, F.L., Zhao, M.Y., 2018. Preparation and properties of ultra-low density proppants for use in hydraulic fracturing. J. Petrol. Sci. Eng. 163, 100–109. https://doi.org/10.1016/ inetrol.2017.10.024
- Fernández, M.E., Baldini, M., Pugnaloni, L.A., Sánchez, M., Guzzetti, A.R., Carlevaro, C.M., 2015. Proppant transport and settling in a narrow vertical wedge-shaped fracture. 49th U.S. Rock Mechanics.
- Gol, R., Wang, C., Gupta, R.B., Yadavalli, V.K., 2017. Synthesis of self-suspending silica proppants using photoactive hydrogels. J. Petrol. Sci. Eng. 157, 651–656. https:// doi.org/10.1016/j.petrol.2017.07.061.
- Hu, X., Wu, K., Li, G., Tang, J., Shen, Z., 2018. Effect of proppant addition schedule on the proppant distribution in a straight fracture for slickwater treatment. J. Petrol. Sci. Eng. 167, 110–119. https://doi.org/10.1016/j.petrol.2018.03.081.
- Huang, X., Yuan, P., Zhang, H., Han, J., Mezzatesta, A., Bao, J., 2017. Numerical study of wall roughness effect on proppant transport in complex fracture geometry. SPE Middle East Oil & Gas Show and Conference. https://doi.org/10.2118/ 183818-MS.
- Jones, A.H., Cutler, R.A., 1985. Hollow Proppants and a Process for Their Manufacture. US Patent No, US4547468.
- Kostenuk, N., Browne, D.J., 2010. Improved proppant transport system for slick-water shale fracturing. In: Canadian Unconventional Resources and International Petroleum Conference. https://doi.org/10.2118/137818-MS.
- Li, J., Kuang, S., Qi, Z., Liu, P., Yu, A., 2022a. Experimental investigation of the leak-off effect on proppant transportation and distribution in a vertical fracture. J. Nat. Gas Sci. Eng. 97, 104358. https://doi.org/10.1016/j.jngse.2021.104358.
- Li, J., Liu, P., Kuang, S., Yu, A., 2021. Visual lab tests: proppant transportation in a 3D printed vertical hydraulic fracture with two-sided rough surfaces. J. Petrol. Sci. Eng. 196, 107738. https://doi.org/10.1016/j.petrol.2020.107738.
- Li, J., Wu, M., Zhou, L., He, S., 2022b. A new proppant type fully coupled fiber-proppant and its property evaluation for unconventional reservoirs. J. Petrol. Sci. Eng. 208, 109573. https://doi.org/10.1016/j.petrol.2021.109573.
- Li, N., Li, J., Zhao, L., Luo, Z., Liu, P., Guo, Y., 2017. Laboratory testing on proppant transport in complex-fracture systems. SPE Prod. Oper. 32, 382–391. https://doi.org/10.2118/181822-PA.
- Li, X., Liao, Z., Yang, Z., Xiong, J., Li, Y., 2018. Stress analysis of hollow proppant based on finite element method. Mater. Sci. Forum 944, 1094—1102. https://doi.org/10.

- 4028/www.scientific.net/MSF.944.1094.
- Li, Y., Zhou, D.H., Wang, W.H., Jiang, T.X., Xue, Z.J., 2020. Development of unconventional gas and technologies adopted in China. Energy Geoscience 1 (1–2), 55–68
- Liao, Z.J., Yang, Z.Z., Xue, Q., Li, X.G., Li, H.B., Li, W.H., 2021. Mechanical behavior of hollow proppants based on finite element model. Energy Sci. Eng. 9, 772–783. https://doi.org/10.1002/ese3.863.
- Mou, J., Xue, Q., Dong, P.P., Li, H., Xu, Y.C., 2017. Preparation and performance of the hollow bauxite ceramic proppant. J. Synth. Cryst. 46, 1244–1249.
 Qu, H., Hu, Y., Liu, Y., Wang, R., Tang, S., Xue, L., 2021a. The study of particle-fluid
- Qu, H., Hu, Y., Liu, Y., Wang, R., Tang, S., Xue, L., 2021a. The study of particle-fluid flow in narrow, curved slots to enhance comprehension of particle transport mechanisms in complex fractures. J. Nat. Gas Sci. Eng. 92, 103981. https:// doi.org/10.1016/j.jngse.2021.103981.
- Qu, H., Tang, S., Liu, Z., McLennan, J., Wang, R., 2021b. Experimental investigation of proppant particles transport in a tortuous fracture. Powder Technol. 382, 95–106. https://doi.org/10.1016/j.powtec.2020.12.060.
- Quintero, H.J., Mattucci, M., Neil, B.O., Folkes, G., Zhang, K., Wang, C.Z., Lu, W., 2018. Enhanced proppant suspension in a fracturing fluid through capillary bridges. In: SPE Western Regional Meeting. https://doi.org/10.2118/190055-MS.
 Tasqué, J.E., Vega, I.N., Marco, S., Raffo, P.A., D'Accorso, N.B., 2020. Ultra-light weight
- Tasqué, J.E., Vega, I.N., Marco, S., Raffo, P.A., D'Accorso, N.B., 2020. Ultra-light weight proppant: synthesis, characterization, and performance of new proppants. J. Nat. Gas Sci. Eng. 85, 103717. https://doi.org/10.1016/j.jngse.2020.103717.
- Wen, Q., Wang, S., Duan, X., Li, Y., Wang, F., Jin, X., 2016. Experimental investigation of proppant settling in complex hydraulic-natural fracture system in shale reservoirs. J. Nat. Gas Sci. Eng. 33, 70–80. https://doi.org/10.1016/j.jngse.2016.05.010.
- Xiao, H., Li, Z., He, S., Lu, X., Liu, P., Li, J., 2021. Experimental study on proppant diversion transportation and multi-size proppant distribution in complex fracture networks. J. Petrol. Sci. Eng. 196, 107800. https://doi.org/10.1016/ j.petrol.2020.107800.
- Xie, X.K., Niu, S.X., Miao, Y., Gao, X., Cheng, L.S., Gao, F., 2019. Preparation and properties of resin coated ceramic proppants with ultra light weight and high strength from coal-series kaolin. Appl. Clay Sci. 183, 105364. https://doi.org/10.1016/j.clay.2019.105364.
- Xu, K., Lu, Y., Chang, J., Weng, D., Li, Y., 2021. Progress of development and application of drag reduction agents for slick-water fracturing. In: Journal of Physics: Conference Series. 2097. https://doi.org/10.1088/1742-6596/2097/1/012022.
- Yao, E., Bai, H., Zhou, F., Zhang, M., Wang, J., Li, F., 2021. Performance evaluation of the multifunctional variable-viscosity slick water for fracturing in unconventional reservoirs. ACS Omega 6, 20822–20832. https://doi.org/10.1021/ acsomega.1c01986.
- Zhang, G., Li, M., Gutierrez, M., 2017. Simulation of the transport and placement of multi-sized proppant in hydraulic fractures using a coupled CFD-DEM approach. Adv. Powder Technol. 28, 1704–1718. https://doi.org/10.1016/j.apt.2017.04.008.
- Zhou, Y., Liu, H., Gao, J.J., Fan, F., Niu, Y.C., Li, S.Z., Mi, Y.Y., Chen, S.Y., Xu, Q., 2022. Coated proppants with self-suspension and tracer slow-release functions. J. Petrol. Sci. Eng. 208. https://doi.org/10.1016/j.petrol.2021.109645.
- Zou, C., Yang, Z., Zhu, R., Zhang, G., Hou, L., Wu, S., Tao, S., Yuan, X., Dong, D., Wang, Y., Wang, L., Huang, J., Wang, S., 2015. Progress in China's unconventional oil gas exploration and development and theoretical technologies. J. Geol. 971. https://doi.org/10.1111/1755-6724.12491.
- Zoveidavianpoor, M., Gharibi, A., 2015. Application of polymers for coating of proppant in hydraulic fracturing of subterraneous formations: a comprehensive review. J. Nat. Gas Sci. Eng. 24, 197–209. https://doi.org/10.1016/j.jngse.2015.03.024.
- Zoveidavianpoor, M., Gharibi, A., bin Jaafar, M.Z., 2018. Experimental characterization of a new high-strength ultra-lightweight composite proppant derived from renewable resources. J. Petrol. Sci. Eng. 170, 1038–1047. https://doi.org/10.1016/j.petrol.2018.06.030.